

# In situ diffraction measurements of lattice response due to shock loading, including direct observation of the $\alpha$ – $\epsilon$ phase transition in iron

D.H. Kalantar<sup>a,\*</sup>, G.W. Collins<sup>a</sup>, J.D. Colvin<sup>a</sup>, J.H. Eggert<sup>a</sup>, J. Hawreliak<sup>b</sup>,  
H.E. Lorenzana<sup>a</sup>, M.A. Meyers<sup>c</sup>, R.W. Minich<sup>a</sup>, K. Rosolankova<sup>b</sup>, M.S. Schneider<sup>c</sup>,  
J.S. Stölken<sup>a</sup>, J.S. Wark<sup>b</sup>

<sup>a</sup>Lawrence Livermore National Laboratory, Livermore, CA 94550, USA

<sup>b</sup>Department of Physics, Clarendon Laboratory, University of Oxford, Oxford OX1 3PU, UK

<sup>c</sup>University of California, San Diego, La Jolla, CA 92093, USA

Available online 31 October 2006

---

## Abstract

In situ diffraction is a technique to probe directly the lattice response of materials during the shock loading process. It is used to record diffraction patterns from multiple lattice planes simultaneously. The application of this technique is described for laser-based shock experiments. The approach to analyze in situ wide-angle diffraction data is discussed. This is presented in the context of single crystal [001] iron shock experiments where uniaxial compression of the bcc lattice by up to 6% was observed. Above the  $\alpha$ – $\epsilon$  transition pressure, the lattice showed a collapse along the [001] direction by 15–18%. Additional diffraction lines appear that confirm the transformation of the iron crystal from the initial bcc phase to the hcp phase.

© 2006 Elsevier Ltd. All rights reserved.

*Keywords:* X-ray diffraction; Laser shocks; Phase transformation

---

## 1. Introduction

When a material experiences shock loading at a very low pressure, it typically responds by deforming elastically. At a pressure above the Hugoniot elastic limit (HEL), stresses that occur in the lattice initiate and propagate dislocations [1,2]. The movement of the dislocations results in rearrangement of the lattice, which is plastic deformation. The number density of dislocations that are generated and the speed with which they propagate depend on the rate of the applied stress, and the energy threshold for the dislocations, which in turn depend on the lattice and its orientation relative to the applied stress.

A standard technique to study the shock response of materials is to measure the rear surface particle speed as the shock releases into either vacuum or an impedance-matched window using a velocity interferometer [3].

---

\*Corresponding author. Tel.: +1 925 422 6147; fax: +1 925 422 8395.

E-mail address: [kalantar1@llnl.gov](mailto:kalantar1@llnl.gov) (D.H. Kalantar).

The rear surface velocity profile is related to the dynamics of the lattice response, providing information on the shock propagation in the solid under dynamic high pressure loading. The specific wave profile depends on properties such as the HEL, the threshold and kinetics of dislocation motion, the magnitude of the shock, and the existence of phase transformations in the pressure range accessed in the experiment.

Identification of features in the wave profiles with physical processes is typically based on a correlation with static high-pressure measurements such as X-ray diffraction. Because high-pressure dynamic loading can markedly affect the structural modifications of solids, such correlations traversing static and dynamic regimes are intrinsically limited in nature. To capture potential complications introduced by lattice kinetics, real-time studies of the lattice are required using a dynamic technique such as in situ X-ray diffraction [4–6]. In situ diffraction provides direct information on the lattice response during shock compression.

High intensity lasers provide a capability to access high-pressure states of material, with diagnostic capabilities that are generally not available on other facilities. Specifically, large lasers with multiple beams provide both a high-pressure capability and simultaneous X-ray diagnostic capability. We have performed a series of experiments using lasers to study the deformation of single crystals by in situ dynamic X-ray diffraction [7–9]. The technique of in situ dynamic diffraction and how it is applied in these laser experiments is described. Key results from shocked single crystal iron experiments are presented as examples [10].

## 2. In situ dynamic diffraction

In situ diffraction has been implemented on laser-based high pressure platforms to provide simultaneous measurements of multiple lattice planes [8,9]. This is a large solid angle measurement of X-rays diffracted from several different lattice planes using a static detector that subtends a large solid angle surrounding the shocked sample. Measurement of the change in lattice spacing of different planes simultaneously provides the detailed information necessary to determine the state of the material under compression, and its deformation.

The target and experimental configuration for in situ diffraction are shown in Fig. 1. The target (Fig. 1a) consists of a single crystal sample, a thin foil used as the source of X-rays for the measurement, and a cylindrical gold shield to protect the detector from direct illumination by the X-ray source. The single crystal sample is coated with a 15–20 mm thick ablation layer of parylene-N and a 0.1 mm aluminum overcoat to prevent shine through of the focused laser beam early in the pulse. A high intensity laser pulse is used to provide the shock loading pressure by direct laser irradiation of the parylene ablation layer. The laser focal spot size that is typically used is 2–3 mm in diameter in order to generate a large area of uniform pressure in the single crystal sample.

Probe X-rays are created by direct laser irradiation of a thin metal foil that is positioned 1–2 mm from the crystal sample. K-shell X-rays are emitted from the hot plasma that is created. A 200 mm diameter pinhole aperture defines the size of the X-ray source. X-rays passing through this aperture diverge spherically from the source and are incident on the single crystal sample at a range of angles, diffracting according to the Bragg diffraction condition:

$$n\lambda = 2d \sin \theta \quad (1)$$

where  $d$  is the lattice spacing,  $\lambda$  the X-ray source wavelength, and  $\theta$  the angle of X-rays relative to the lattice plane, as shown in Fig. 2.

When the lattice undergoes a deformation due to the shock loading, the spacing of the lattice planes change. Provided the range of incidence angles for the X-rays is large enough to meet the Bragg condition for both the uncompressed and compressed lattice spacings, X-rays will diffract from both lattice configurations. Since the source of X-rays is located close to the single crystal sample, the Bragg condition may be met for several different lattice planes simultaneously.

A large area segmented film holder is positioned surrounding the target, subtending up to a full  $\pi$ -steradian solid angle (Fig. 1b). This detector intercepts X-rays that are diffracted from the many different lattice planes, resulting in an image of diffraction curves, such as shown in Fig. 3. Here, diffraction curves from different lattice planes of shocked single crystal [001] iron recorded at a range of loading pressures are shown. By varying the timing of the probe relative to the pressure drive, diffraction curves from both the unshocked and shocked lattice may be recorded on the same film. Several curves in the images in Fig. 3 show shifted features

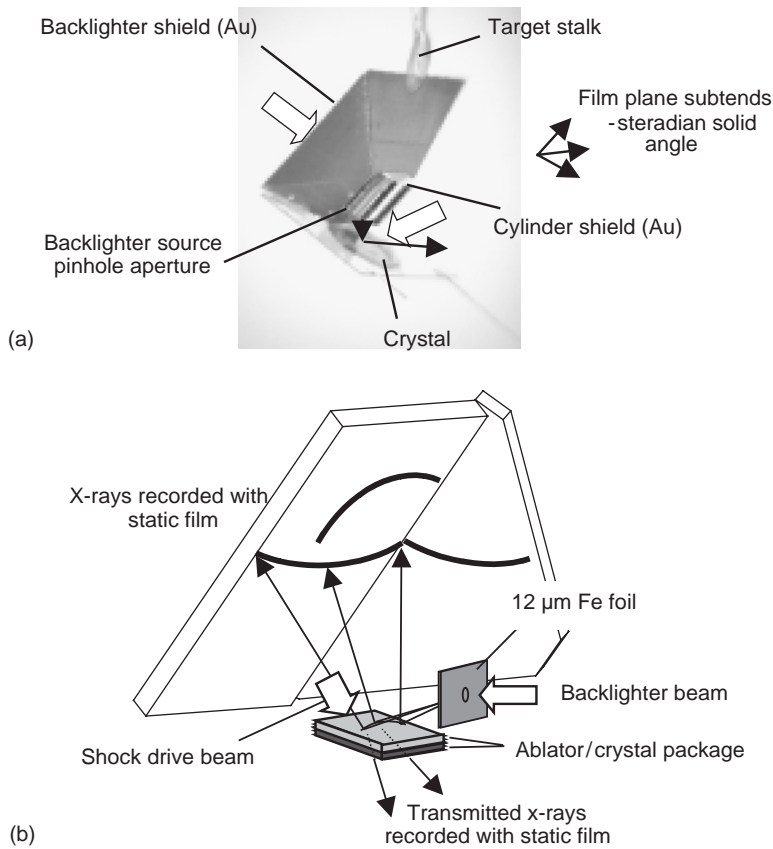


Fig. 1. (a) Example target showing the crystal and backlighter foil components. (b) Geometry for in situ wide-angle diffraction measurements showing the large angle coverage of the film detector.

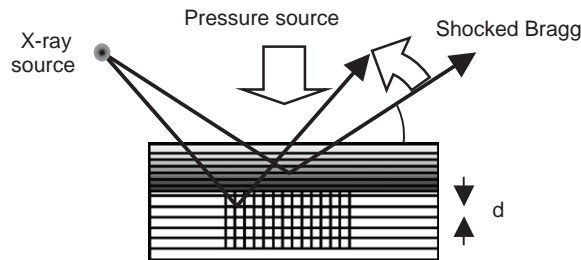


Fig. 2. Geometry for in situ Bragg diffraction. X-rays are incident at a wide angle, satisfying the Bragg condition for different lattice spacings at different locations in the crystal. The diffracted signal shifts at the detector due to compression of the lattice.

due to the shock loading of the crystal. However, not all curves show evidence of compression since these curves result from X-rays diffracting from different spatial locations on the sample. When these regions fall outside the area on the crystal that is shock loaded, the shifted curves do not appear. This is discussed below.

### 3. Approach for analysis

In the example of diffraction from a lattice plane that is parallel to the surface of the crystal, such as the (002) plane of [001] Fe, the Bragg condition is met on a circular arc on the surface of the crystal, and a cone of X-rays is diffracted, intercepting the film in a conic section. However, more generally the lattice planes are not parallel to the surface of the crystal. The effective probe depth for the X-rays is typically only a few microns.

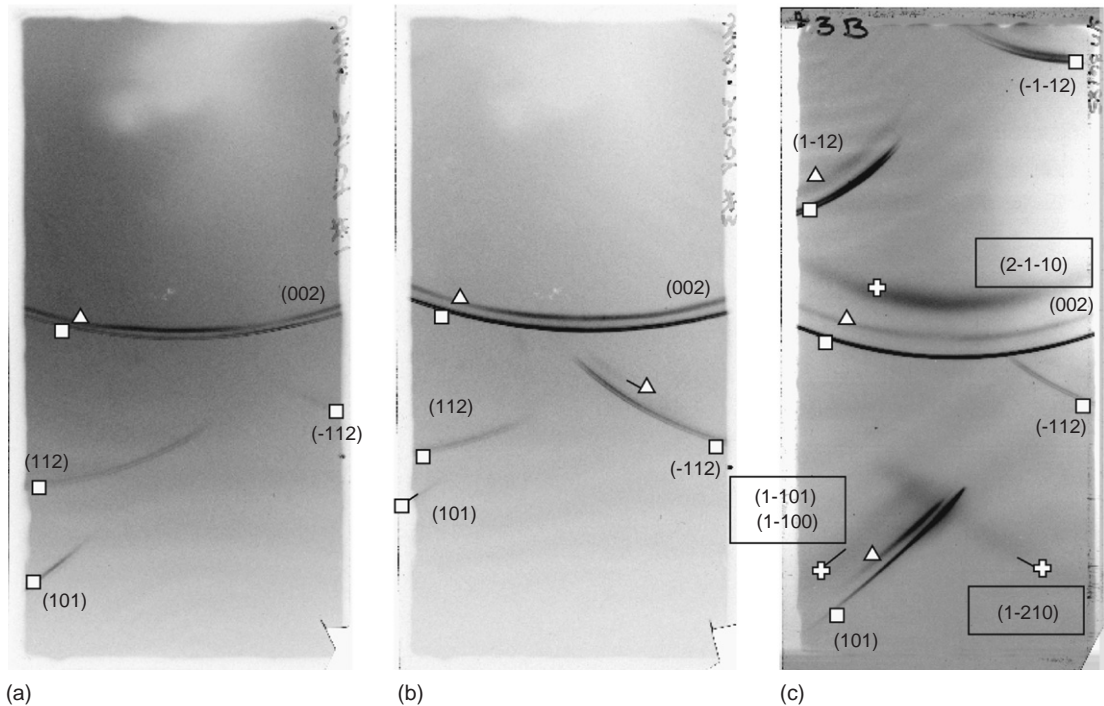


Fig. 3. Example film images showing multiple plane diffraction from single crystal [001] iron recorded at laser intensities of: (a)  $2.0 \times 10^{10} \text{ W/cm}^2$  at 532 nm (1.3 GPa); (b)  $6.0 \times 10^{10} \text{ W/cm}^2$  at 532 nm (3.8 GPa); and (c)  $3.1 \times 10^{10} \text{ W/cm}^2$  at 351 nm irradiation (26 GPa). The diffraction lines from the static lattice are identified with squares, lines from the uniaxial compressed lattice are identified with triangles, and lines corresponding to the hcp phase are identified with crosses.

As a result, the region on the crystal that meets the Bragg condition cannot be approximated by a single cone of X-rays, and it is necessary to include the detailed source and sample geometry in interpreting the film images.

Software routines have been developed to calculate the diffraction pattern for the laser experiments where the monochromatic X-ray source is located close to the crystal. One such approach is described here. The crystal surface is represented by a grid of points. A bundle of rays from the X-ray source to the grid of points on the crystal surface (pixels) are calculated for a given lattice plane defined by  $h, k, l$  indices. The direction of reflection off the lattice plane is calculated for each ray. These rays are then propagated to the film plane. The intersection each rays with the film plane is calculated in coordinates representing position in the plane of the film.

An image is created to represent the locations on the crystal where the Bragg diffraction condition is met. This is defined with an intensity  $Y$ :

$$Y \propto \exp \left[ -\frac{\delta n \lambda}{2d \sin \theta} \right] \frac{a^2}{\lambda^2} \quad (2)$$

where  $\lambda$  is the wavelength of probe X-rays,  $d$  the lattice spacing, and  $\theta$  the angle of the X-rays relative to the lattice plane. A representative line width  $a$  is applied to generate narrow curves on the crystal corresponding to where the diffraction occurs (where  $\theta$  is equal to the Bragg angle). This image has a value of 1 at locations on the crystal where the Bragg condition is met, and 0 elsewhere. This map of where diffraction occurs on the crystal is then mapped to the film plane coordinates as defined by the ray tracing from each point on the crystal, resulting in a simulated film image of diffraction from the given  $h, k, l$  lattice plane. This is repeated for the different  $h, k, l$  indices that are allowed for the given crystal symmetry to create a simulated diffraction film image.

An example is shown for single crystal iron in Fig. 4. Here, we show the calculated image due to  $1.85 \text{ \AA}$  X-rays that are diffracted from the (002) and (7 17 12) and (7 101) lattice planes of static (uncompressed) [001] iron crystal. The image showing where diffraction occurs on the crystal is shown in Fig. 4a, and the corresponding simulated film image is shown in Fig. 4b. Note that the extent of the diffraction lines in the film image is determined by the size and orientation of the crystal.

Diffraction patterns are calculated for the static lattice, and compared with the experimental film images in order to determine the specific geometry of the target and film for each experiment. Patterns are then calculated assuming different lattice deformations to compare with the diffraction curves due to the compressed lattice. In order to make this comparison, a range of different configurations may be considered by varying the dimension and rotation of the crystal in the simulation.

In the example of [001] Fe, the (002) planes are parallel to the shock loading direction. The compression of the lattice in this direction is determined directly from the shift of the diffraction curve from the (002) planes. Determination of whether the lattice compression is purely uniaxial or hydrostatic is based on comparison of the film data with simulated images that assume compression of the lattice in the perpendicular directions as well. The pattern from static (uncompressed) iron is shown in Fig. 5a, with additional features overlaid that were calculated based on uniaxial compression of the initial bcc lattice by 0.95 along [001]. The same image calculated assuming that the crystal is compressed by 0.95 along all three lattice directions is shown in Fig. 5b. This would be the case for a lattice that plastically deformed due to the generation and propagation of dislocations.

The test cases that are shown in Fig. 5 illustrate the sensitivity of the shifted diffraction lines to the lattice deformation. The relative shift of the diffraction curves from different lattice planes provides a quantitative measure of the overall lattice deformation—whether it undergoes uniaxial compression, or there is a relaxation that results in compression perpendicular to the shock direction. Comparison of the relative shifts of the different diffraction curves may also indicate a rotation of the lattice, and the appearance or disappearance of diffraction curves may be an indication of a phase change in the structure of the lattice.

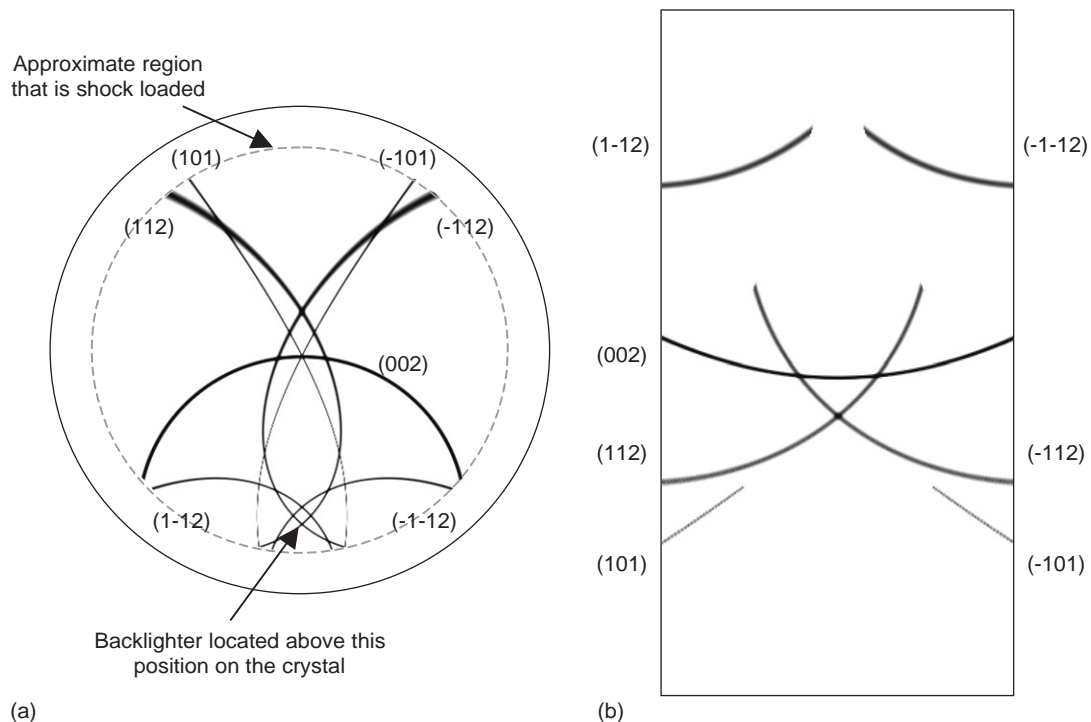


Fig. 4. (a) Simulated image showing locations on the crystal where diffraction occurs from several different lattice planes. (b) Simulated film image showing the locations of the diffraction curves. These sample images are simulated for a single crystal [001] iron lattice with iron K-shell X-rays at  $1.85 \text{ \AA}$ .

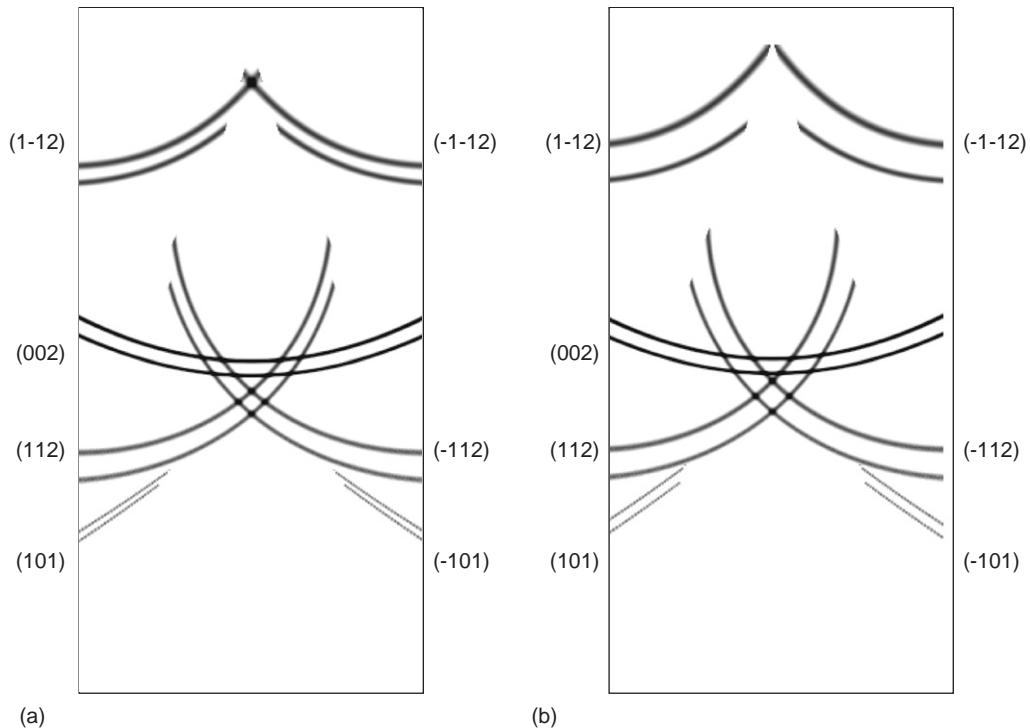


Fig. 5. Simulated film image showing diffraction from: (a) static and uniaxially compressed bcc lattice, and (b) static and hydrostatically compressed bcc lattice. The overall deformation of the lattice affects the shift of each line differently.

This approach of simulating the diffraction pattern based on initial assumptions of the lattice configuration provides insight into the response of a material to pressure loading. A more general analysis capability is being developed where the peak positions of each diffraction curve are identified, and the overall lattice deformation is calculated based on an optimum fit.

#### 4. Shock experiments in single crystal iron

The technique of in situ dynamic X-ray diffraction has been used to probe shocked single crystals with X-rays as they undergo deformation by shock compression. Experiments have been done previously to study shocked silicon and copper [7,9]. Recent experiments have focused on the deformation of single crystal iron [10]. We present analysis of the shocked iron experiments to illustrate the analysis of the in situ diffraction measurement. In these experiments, features in the diffraction data are consistent with an initial uniaxial compression and subsequent collapse and transformation from the bcc phase to the hcp phase.

Previously, the presence of a phase transformation in shock-loaded iron was identified at 13 GPa based on the observation of structure in wave profile measurements [11,12]. Separately, a solid–solid phase transformation in iron under static loading conditions was observed at the same pressure [13]. The correlation of the static measurement with the dynamic loading result was taken as evidence that iron undergoes this solid–solid transition on shock loading. This is supported by microstructural analysis of the residual deformation in recovered samples [14,15], but direct confirmation of this transition during shock loading requires in situ measurements.

Single crystal iron samples were prepared with a 16 mm thick parylene ablation layer, and a 0.1 mm overcoat of aluminum. A single beam of OMEGA [16] or Janus was used to irradiate the single crystal samples with a 2–6 ns flat-in-time laser pulse shape. Additional laser beams were used to create a bright source of X-rays

by direct laser irradiation of a thin iron foil located at 1.3 mm from the center of the crystal. X-rays diffracted from the shocked single crystal were recorded with static film. Additional experiments were conducted at the Vulcan laser [17], with similar thick crystals, as well as with much thinner 10  $\mu$ m single crystal iron foils [10].

The single crystals were subjected to a high intensity pressure drive by direct laser irradiation at intensities of approximately  $2 \times 10^{10}$ – $5 \times 10^{11}$  W/cm<sup>2</sup> at 351–1056 nm wavelength. At these low intensities, LASNEX [18] simulations of the laser interaction with the Al-coated CH suggested that the pressure scales nearly linearly with intensity. In addition, simulations with 351 and 532 nm laser wavelength provided a scale factor of 0.76 to relate the 532 nm laser intensities to the 351 nm intensities and a scale factor of 0.30 to relate the 1054 nm laser intensities to the 351 nm intensities. The absolute pressures achieved in these experiments were determined based on third-order elasticity constants [10].

The deformation of the iron lattice was recorded at a range of laser intensities. Three examples of the diffraction data are shown in Fig. 3. In each image, there are multiple diffraction curves present, each resulting from X-rays diffracted from a single lattice plane. Several of the lattice planes show both static and compressed features. Since the crystals were cut with a [001] orientation, the shift of the (002) diffraction line provides a direct measurement of the lattice compression along the shock propagation direction.

The precise geometry for the source, crystal, and film planes were determined for each image to match the diffraction lines from the uncompressed lattice planes. The relative shift of the diffraction from the different lattice planes were then compared with calculations such as those shown in Fig. 5 under a range of lattice deformation conditions. The compression of different lattice planes observed in Figs. 3a and b are consistent with an overall uniaxial compression of the initially bcc lattice. The shift of lattice planes that are at an angle with respect to the shock direction are consistent with an overall compression of the lattice only along the [001] direction as indicated by the shift of the (002) diffraction.

In the case of the film image recorded at higher pressure shown in Fig. 3c, multiple compressions are evident. Several lattice planes show a shift that is consistent with a nearly uniaxial compression of the lattice by 6% along the [001] direction (parallel to the shock). Additional broader curves appear at a larger offset. Most of these additional diffraction curves are consistent with 15–18% compression of the lattice along the shock direction. However, one additional diffraction curve appears that cannot be explained with the symmetry of the compressed bcc lattice. This additional diffraction curve is consistent with diffraction from the (1–210) plane of hcp iron. Other film images were recorded showing other hcp planes, confirming that iron undergoes a solid–solid transformation on the ns time-scale of these laser shock experiments.

The relative positions of the different diffraction lines from the hcp lattice constrain the lattice unit cell. In Fig. 3c, the collapse of the initially bcc lattice is evident by the broad shifted lines adjacent to the (002) and (101) diffraction curves. These are consistent with planes in uniaxially compressed bcc and are also identified with the hcp structure. The combination of these diffraction curves and the appearance of the additional (1–210) hcp line are consistent with the uniaxial collapse of the bcc structure and shuffle of alternate [110] planes of atoms [10].

The measured compression of the lattice along the [001] direction is plotted as a function of laser intensity in Fig. 6. In this figure, the compression was determined from the shift of the (002) diffraction curve. The lattice deformation is uniaxial along the shock direction at low intensity and the plane spacing decreases with increasing laser intensity (pressure) to a maximum relative compression of 0.94.

At laser intensities above approximately  $1.5 \times 10^{11}$  W/cm<sup>2</sup>, two shifted diffraction curves are evident in the film images. The uniaxial compression feature maintains a fixed shift corresponding to approximately 0.94 compression for a range of laser intensities. The second shifted curve is consistent with 15–18% compression of the initial bcc lattice. Both compressions are shown in the figure. The open symbols represent the low compression observed in images that also showed a corresponding higher compression (solid symbols). This discontinuous behavior is consistent with a volume collapse and transformation of the initially bcc structure to the hcp structure. The presence of both compressions simultaneously is assumed to be due to a two-wave structure in the shock. The X-ray measurements are time-integrated over 1–3 ns, during the shock loading of the iron crystal.

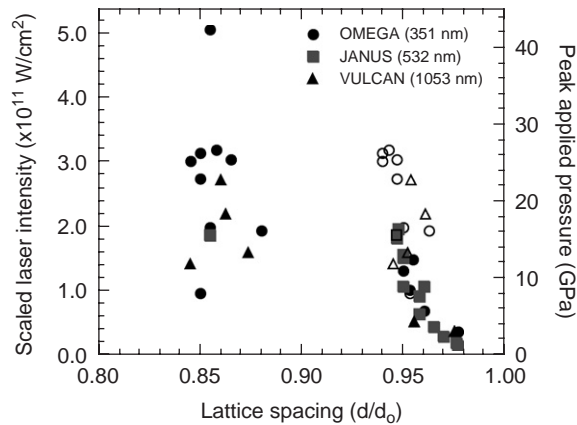


Fig. 6. Compression of the lattice as a function of laser irradiation intensity (pressure) determined by the shift of the (002) diffraction curves. For images that showed low and high compressions on the same film record, both compressions are indicated. The open symbols represent the lower compression.

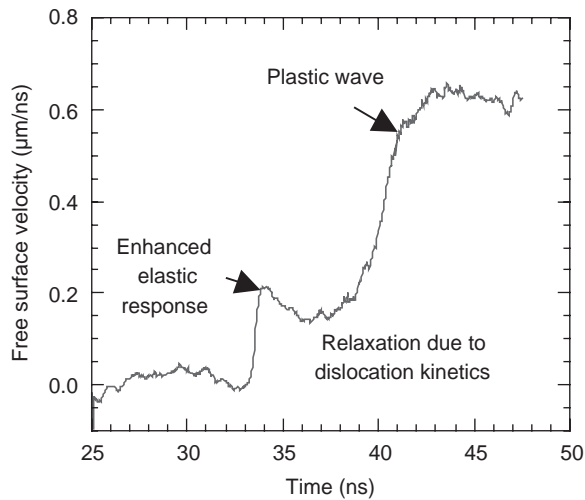


Fig. 7. VISAR free surface wave profile of the breakout from [001] single crystal iron.

## 5. Pressure calibration

The lattice compression measurements shown in Fig. 6 are plotted both as a function of intensity and pressure. The pressure scale that is shown is based on third-order elasticity constants. At low intensity where only a single compression of the (002) planes was observed, the shift of the diffraction curves from each lattice plane was consistent with an overall uniaxial compression of the lattice. Third-order elasticity constants for iron [19,20] were used to determine the pressure corresponding to the uniaxial lattice deformation for each low pressure image. The average scale factor from laser intensity to pressure for all such low pressure measurements was applied to determine a pressure for each data point. This mean scale factor had a 10% statistical error.

The pressure scale determined based on third-order elasticity constants is consistent with the shock Hugoniot for iron and the phase transformation at 13 GPa. Free surface wave profile measurements of these shocked crystals were made, such as shown in Fig. 7. This shows an example wave profile from a 250  $\mu\text{m}$  thick single crystal [001] iron sample that was shock-loaded by direct laser irradiation. This is a spatially averaged lineout from a line imaging VISAR. In this case, the peak loading pressure was approximately 40 GPa. The wave decayed to approximately 7.5 GPa at the back surface of the sample. The wave profile

shows a two-wave structure due to the elastic and plastic waves. The elastic response is enhanced relative to the HEL for iron, due to the low initial dislocation density and kinetics of generating and propagating dislocations. Modeling of these waveforms is ongoing using the LASNEX hydrodynamics code and also using a kinetics model [21,22].

## 6. Conclusions

Shock experiments provide information on the mechanical properties of materials, including the elastic response, plastic deformation, equation of state, and phase transformations. Laser-based shock experiments have been developed to characterize the response of materials under high pressure and high strain rate conditions.

One diagnostic technique that has been applied to laser shock experiments is in situ diffraction. This technique utilizes a laser-produced plasma as a source of monochromatic X-rays incident on a sample crystal that is shock loaded by direct laser irradiation. X-rays that diffract from the shocked sample are recorded during shock loading using a wide-angle detector. This ensures that when the diffraction lines shift due to deformation of the lattice, the shifted lines are captured on the detector. The amount of shift of the different lattice planes provides information on the deformation of the lattice as it deforms. Time resolution of these measurements provides information on the dynamics of the lattice deformation.

The technique of in situ diffraction has been used to study the response of single crystal [001] iron to shock loading. At low pressures, the iron responds with a nearly uniaxial deformation with a compression of up to 6% along the shock direction. This maximum compression corresponds to shock loading just below the  $\alpha$ - $\epsilon$  transformation pressure of 13 GPa. Above this pressure, both a uniaxial compression by 6% and a collapse and transformation to hcp are observed. Both states are observed due to the two-wave response of the lattice. These results provide direct confirmation of the hcp phase during the ns time-scale of the laser shock experiments.

## Acknowledgements

This work was conducted under the auspices of the US Department of Energy by the University of California Lawrence Livermore National Laboratory under Contract no. W-7405-Eng-48. Experiments were conducted at the University of Rochester Laboratory for Laser Energetics under the NLUF grants program. Additional support was provided by the Department of Energy under Grants DEFG0398DP00212 and DEFG0300SF2202, by the UK EPSRC under Grant GR/R25699/01, and by LDRD 04-ERD-071 at LLNL.

## References

- [1] Zaretsky E. Dislocation multiplication behind the shock front. *J Appl Phys* 1995;78:3740.
- [2] Chhabildas LC, Asay JR. Rise time measurements of shock transitions in aluminium, copper, and steel. *J Appl Phys* 1979;50:2749.
- [3] Barker LM, Hollenbach RE. Laser interferometer for measuring high velocities of any reflecting surface. *J Appl Phys* 1972;43:4669.
- [4] Johnson Q, Mitchell A, Evans L. *Nature (London)* 1979;231:310;  
Johnson Q, Mitchell A, Evans L. *Appl Phys Lett* 1972;21:29.
- [5] Wark JS, Whitlock RR, Hauer AA, Swain JE, Solone PJ. Subnanosecond X-ray diffraction from laser-shocked crystals. *Phys Rev B* 1989;40:5705.
- [6] Rigg PA, Gupta YM. Real-time X-ray diffraction to examine elastic-plastic deformation in shocked lithium fluoride crystals. *Appl Phys Lett* 1998;73:1655.
- [7] Loveridge-Smith A, Allen A, Belak J, Boehly T, Hauer A, Holian B, et al. Anomalous elastic response of silicon to uniaxial shock compression on nanosecond timescales. *Phys Rev Lett* 2001;86:2349.
- [8] Kalantar D, Bringa E, Caturla M, Colvin J, Lorenz KT, Kumar M, et al. Multiple film plane diagnostic for shocked lattice measurement. *Rev Sci Instrum* 2003;74:1929.
- [9] Kalantar D, Belak J, Bringa E, Budil K, Caturla M, Colvin J, et al. High pressure, high strain rate lattice response of materials. *Phys Plasmas* 2003;10:1569.
- [10] Kalantar D, Belak J, Collins GW, Colvin JD, Davies HM, Eggert JH, et al. Direct observation of the  $\alpha$ - $\epsilon$  transition in shock-compressed iron via nanosecond X-ray diffraction. *Phys Rev Lett* 2005;95:075502.
- [11] Walsh JM. *Bull Am Phys Soc* 1954;29:28.

- [12] Bancroft D, Peterson L, Minshall S. Polymorphism of iron at high pressure. *J Appl Phys* 1956;27:291.
- [13] Jamieson JC, Lawson AW. X-ray diffraction studies in the 100 kilobar pressure range. *J Appl Phys* 1962;33:776.
- [14] Smith CS. *Trans Metall Soc AIME* 1958;214:574.
- [15] Sano T, Mori H, Ohmura E, Miyamoto I. Femtosecond laser quenching of the epsilon phase of iron. *Appl Phys Lett* 2003;83:3498.
- [16] Boehly TR, Craxton RS, Hinterman TH, Kelly JH, Kessler TJ, Kumpan SA, et al. The upgrade to the OMEGA laser system. *Rev Sci Instrum* 1995;66:508.
- [17] Danson CN, Barzanti L, Chang Z, Damerell AE, Edwards CB, Hancock S, et al. High contrast multi-terawatt pulse generation using chirped pulse amplification on the VULCAN laser facility. *Opt Commun* 1993;103:392.
- [18] Zimmerman GB, Kruer W. Numerical simulation of laser-initiated fusion. *Comments Plasma Phys Control Fus* 1975;2:51.
- [19] Landolt-Bornstein. Numerical data and functional relationships in science and technology—Group III. *Cryst Solid State Phys* 1979;0:11.
- [20] Ritchie AD. Anharmonicity in alpha-iron: the third order elastic coefficients. PhD thesis, University of California at Davis, January 1969, and LLNL Technical Document, UCRL-50548, 1969.
- [21] Colvin JD, Kalantar D. Scaling of pressure with intensity in laser-driven shocks and effects of hot X-ray preheat. In: *Proceedings of the 2005 APS topical conference on shock compressed condensed matter*, Baltimore, MD, USA, 2005.
- [22] Gilman JJ. Microdynamics of plastic flow at constant stress. *J Appl Phys* 1965;36:2772.